Periradicular tissue fluid-derived biomarkers for apical periodontitis

Virdee, Satnam S.; Bashir, Nasir Z.; Krstic, Milan; Camilleri, Josette; Grant, Melissa M.; Cooper, Paul R.; Tomson, Phillip L.

DOI:
10.1111/iej.13956

Received: 15 March 2023 | Accepted: 14 July 2023

DOI: 10.1111/iej.13956

INTERNATIONAL ENDODONTIC JOURNAL | WILEY

ORIGINAL ARTICLE

Periradicular tissue fluid-derived biomarkers for apical periodontitis: An *in vitro* methodological and *in vivo* cross-sectional study

Satnam S. Virdee[1] | **Nasir Z. Bashir**[2] | **Milan Krstic**[1] | **Josette Camilleri**[1] | **Melissa M. Grant**[1] | **Paul R. Cooper**[3] | **Phillip L. Tomson**[1]

[1]Institute of Clinical Sciences, School of Dentistry & Birmingham Dental Hospital, University of Birmingham, Birmingham, UK

[2]School of Dentistry, University of Leeds, Leeds, UK

[3]Department of Oral Sciences, Faculty of Dentistry, University of Otago, Dunedin, New Zealand

Correspondence
Satnam S. Virdee, Institute of Clinical Sciences, The University of Birmingham School of Dentistry, Edgbaston, Birmingham B5 7EP, UK.
Email: s.s.virdee.1@bham.ac.uk

Funding information
British Endodontic Society; European Society of Endodontology; Oral & Dental Research Trust

Abstract

Background: Periradicular tissue fluid (PTF) offers a source of diagnostic, prognostic and predictive biomarkers for endodontic disease.

Aims: (1) To optimize basic parameters for PTF paper point sampling *in vitro* for subsequent *in vivo* application. (2) To compare proteomes of PTF from teeth with normal apical tissues (NAT) and asymptomatic apical periodontitis (AAP) using high-throughput panels.

Methodology: (1) To assess volume absorbance, paper points ($n = 20$) of multiple brands, sizes and sampling durations were inserted into PBS/1%BSA at several depths. Wetted lengths (mm) were measured against standard curves to determine volume absorbance (μL). To assess analyte recovery, paper points ($n = 6$) loaded with 2 μL recombinant IL-1β (15.6 ng/mL) were eluted into 250 μL: (i) PBS; (ii) PBS/1% BSA; (iii) PBS/0.1% Tween20; (iv) PBS/0.25 M NaCl. These then underwent: (i) vortexing; (ii) vortexing/centrifugation; (iii) centrifugation; (iv) incubation/vortexing/centrifugation. Sandwich-ELISAs determined analyte recovery (%) against positive controls.

(2) Using optimized protocols, PTF was retrieved from permanent teeth with NAT or AAP after accessing root canals. Samples, normalized to total fluid volume (TFV), were analysed to determine proteomic profiles (pg/TFV) of NAT and AAP via O-link Target-48 panel. Correlations between AAP and diagnostic accuracy were explored using principal-component analysis (PCA) and area under receive-operating-characteristic curves (AUC [95% CI]), respectively. Statistical comparisons were made using Mann–Whitney *U*, ANOVA and *post hoc* Bonferonni tests ($\alpha < .01$).

Results: (1) UnoDent's 'Classic' points facilitated maximum volume absorbance ($p < .05$), with no significant differences after 60 s (1.6 μL [1.30–1.73]), 1 mm depth and up to 40/0.02 (2.2 μL [1.98–2.20]). For elution, vortexing (89.3%) and PBS/1% BSA (86.9%) yielded the largest IL-1β recovery ($p < .05$).

(2) 41 (NAT: 13; AAP: 31) PTF samples proceeded to analysis. The panel detected 18 analytes (CCL-2, -3, -4; CSF-1; CXCL-8, -9; HGF; IL-1β, -6, -17A, -18; MMP-1,

-12; OLR-1; OSM; TNFSF-10, -12; VEGF-A) in ≥75% of AAP samples at statistically higher concentrations ($p < .01$). CXCL-8, IL-1β, OLR-1, OSM and TNFSF-12 were strongly correlated to AAP. 'Excellent' diagnostic performance was observed for TNFSF-12 (AUC: 0.94 [95% CI: 0.86–1.00]) and the PCA-derived cluster (AUC: 0.96 [95% CI: 0.89–1.00]).

Conclusions: Optimized PTF sampling parameters were identified in this study. When applied clinically, high-throughput proteomic analyses revealed complex interconnected networks of potential biomarkers. TNFSF-12 discriminated periradicular disease from health the greatest; however, clustering analytes further improved diagnostic accuracy. Additional independent investigations are required to validate these findings.

KEYWORDS

absorbance, apical periodontitis, biomarkers, elution, inflammation, periradicular tissue fluid

INTRODUCTION

Periradicular tissue fluid (PTF) is an interstitial fluid derived from the vasculature surrounding the root of a tooth (Nair, 2004). In normal apical tissues (NAT), this serum is transudative and accumulates within extracellular spaces via passive diffusion across osmotic gradients. Stimulation from endodontic pathogens, however, initiates a localized inflammatory response that encourages fluid extravasation by increasing capillary membrane permeability (Hama et al., 2006; Ricucci & Bergenholtz, 2004). In this diseased state, such as asymptomatic apical periodontitis (AAP), PTF is considered an inflammatory exudate that progressively becomes enriched with autocrine and paracrine signalling molecules (Márton & Kiss, 2000). These pro- and anti-inflammatory peptides are responsible for orchestrating a myriad of cellular events involved in local tissue destruction and the development of clinical symptoms (Márton & Kiss, 2014).

In recent years, PTF has been retrieved clinically through root canals using paper points and its composition investigated at the proteomic and transcriptomic levels (Virdee et al., 2019). These experiments have quantified analytes (Martinho et al., 2016; Safavi & Rossomando, 1991; Shimauchi et al., 1996), correlated them with acute endodontic symptoms (Alptekin et al., 2005; Martinho et al., 2016; Pezelj-Ribarić et al., 2007), longitudinally monitored changes throughout treatment (Alptekin et al., 2005; Grga et al., 2013; Liu et al., 2003) and utilized several markers as surrogate outcome measures in clinical trials (Corazza et al., 2021; Teixeira et al., 2022; Zhi et al., 2017). This body of evidence demonstrates PTF's ability to be harvested for local biomarker molecular analysis and proof-of-concept for their diagnostic, prognostic and predictive potential. Thus, a noninvasive chairside sampling procedure targeting individual or groups of analytes could provide clinicians with more sensitive and specific information regarding periradicular disease status than currently available diagnostic techniques (Dummer et al., 1980; Klausen et al., 1985; Lofthag-Hansen et al., 2007). Similar studies have already identified biomarkers within other oral exudates, notably Matrix Metallopeptidase [MMP]-8 in gingival crevicular fluid (GCF) for use in periodontal disease diagnosis (Sorsa et al., 2020).

Despite recent progress, there still remains an absence of universal protocols for sampling PTF. This could be due to a lack of methodological work-up data, which contrasts other intricate diagnostic procedures where basic parameters have been first optimized *in vitro* (Hartroth et al., 1999; Inic-Kanada et al., 2012; Zehnder et al., 2014). Additionally, existing PTF studies have limited their investigations to a small array of cytokines using conventional enzyme-linked immunosorbent assays (ELISA; Rechenberg et al., 2014; Teixeira et al., 2022; Zhi et al., 2017). It thus remains one of the only oral exudates that has not been characterized using more contemporary high-throughput methods of proteomic analysis, an approach that better reflects the complex multifaceted nature of periradicular pathophysiology. Furthermore, whilst 45 PTF-derived mediators have been detected across 33 studies (Virdee et al., 2019), data pertaining to their diagnostic performance has yet to be reported. This analysis would be required for determining those individual or molecular groups that could reliably serve as biomarkers for different periradicular disease states, for which there is currently no consensus.

AIMS

In order to enhance PTF retrieval for the *in vivo* cross-sectional study an *in vitro* methodological study was

conducted. The primary aims of the *in vitro* study were to determine the basic parameters facilitating (1) maximum volume absorbance and (2) analyte recovery during paper point sampling of PTF. The primary aim of the *in vivo* cross-sectional study was to use the optimized sampling protocol to identify potential biomarkers for AAP by comparing the proteome of PTF from teeth diagnosed with NAT or AAP. Secondary *in vivo* objectives included (1) exploring associations between peptides and disease states to identify distinct clusters of biomarkers, or biosignatures, for AAP and (2) determining the diagnostic performance of PTF-derived mediators in discriminating periradicular disease from health.

The null hypotheses tested were: (i) different paper point brand, size and sampling durations do not significantly influence absorbed volume; (ii) eluting buffer and technique do not significantly influence analyte recovery; (iii) there are no significant differences in PTF analyte concentrations between NAT and AAP.

MATERIALS AND METHODOLOGY

This study was performed in accordance with 2021 Preferred Reporting Items for Laboratory studies in Endodontology (PRILE) and 2023 Preferred Reporting items for Observational studies in Endodontics (PROBE) guidelines (Nagendrababu et al., 2021, 2023; Figure 1). Ethical approval was attained from the University of Birmingham's Dentistry Research Tissue Bank (19/SW/0198) for obtaining PTF as part of routine treatment. Informed consent to retain waste tissue was documented in the participant's electronic medical records.

In vitro methodological studies

Volume absorbance

The laboratory model previously described by Shimauchi et al. (1996), which explored the relationship between fluid volume and paper point wetted length, was adapted to determine the optimal parameters for PTF absorbance. Briefly, paper points from five independent batches were pooled into a polythene bag in accordance with their size and brand and subsequently coded for operator blinding. They were then randomly selected from each bag and with locking college tweezers, perpendicularly clasped at prespecified lengths from their tips depending on the desired insertion depth. These were then suspended within 1.5 mL microfuge tubes (Thermo Fisher Scientific) containing 500 μL phosphate-buffered saline (PBS) and 1% bovine serum albumin (BSA; Sigma-Aldrich), which acted as an *in vitro* substitute for PTF. To improve stability, the gripping component of tweezers was firmly rested upon the coronal aspect of the open microfuge tube, which in itself was supported in a microtube rack. Absorbed volume (μL) was then immediately calculated using a predetermined wetted length (mm) to volume (μL) standard curve. All measurements, including those for testing the parameters below, were taken under magnification using a 0.5 mm graduated stainless-steel ruler. The following parameters, all selected for their use in prior PTF studies, were evaluated using sample sizes consistent with other similar investigations ($n = 20$; Pumarola-Suñé et al., 1998; Shimauchi et al., 1996):

(i) Brand: Classic (UnoDent), DeTrey (Densply Sirona), DiaDent, HS Maxima (Henry Schein), Maillefer, Orbis, Panadent, QED, Roeko Colour, SybronEndo (Kerr Dental) and VDW tested using 15/0.02 cones for 60 s and 1 mm insertion depth. The brand yielding the greatest absorbance was used in subsequent investigations.
(ii) Insertion depth: 1-, 2-, 3- and 4-mm insertion depths tested using 15/0.02 cones for 60 s.
(iii) ISO size: 15/0.02, 20/0.02, 30/0.02 and 40/0.02 cones tested for 60 s at 1 mm insertion depth.
(iv) Sampling duration: 30, 60, 90 and 120 s tested using 15/0.02 cones at 1 mm insertion depth.

Analyte recovery

The laboratory model previously described by Inic-Kanada et al. (2012), which compared cytokine recovery of different ophthalmic sponges and solutions, was adapted to determine eluting efficacy of several buffers and techniques employed in prior PTF studies. Briefly, recombinant Interleukin [IL]-1β (Bio-Techne), used as a representative analyte (Shimauchi et al., 1996), was reconstituted to 15.6 ng/mL in PBS/1% BSA (Sigma-Aldrich). Two microlitres were loaded onto a single 15/0.02 cone via calibrated pipettor (Gilson), which was then inserted into a 1.5 mL microfuge tube containing 250 μL of: (i) PBS; (ii) PBS/1% BSA; (iii) PBS/0.1% Tween20; (iv) PBS/0.25 M Sodium Chloride (NaCl). These then underwent elution via:

(i) 1 min vortex (Starlab Ltd)
(ii) 1 min vortex (Starlab Ltd) and 10 min centrifugation (Eppendorf) at 5000 *g* at 4°C
(iii) 10 min centrifugation (Eppendorf) at 5000 *g* at 4°C
(iv) 300 min incubation at room temperature, 1 min vortex and 10 min centrifugation (Eppendorf) at 5000 *g* at 4°C

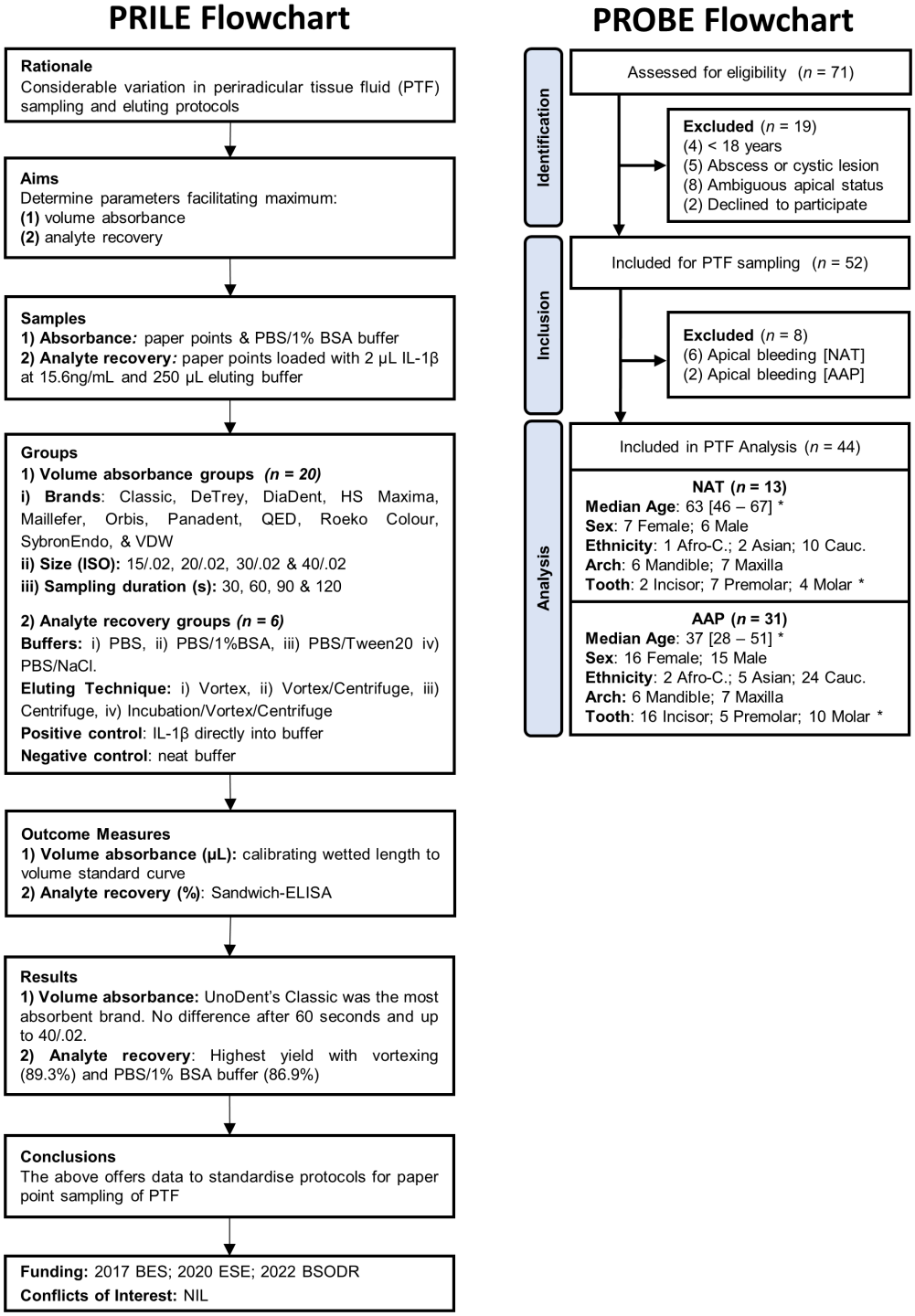

FIGURE 1 PRILE and PROBE flowcharts. *$p < .05$.

Under these conditions, 100% analyte recovery equated to 125 pg/mL and the median of the standard curve. For positive controls, 2 µL reconstituted IL-1β was inserted directly into buffers whereas neat solutions served as negative controls. Each group had sample sizes consistent with other experiments investigating analyte recovery ($n = 6$; Inic-Kanada et al., 2012). The resulting buffer containing the single loaded cone was then collected, coded for operator blinding and stored at −20°C until analysis. This was performed using a standard commercial IL-1β sandwich-ELISA kit (Bio-Techne) in accordance with the manufacturer's instructions. Briefly, 100 µL test, control and standard samples were added in duplicates to a clear flat bottom 96-well plate after coating with IL-1β specific monoclonal capture antibody and blocking with the reagent diluent provided. After 2 h of incubation at room temperature,

100 μL IL-1β polyclonal antibody conjugated to horseradish peroxidase was added to each well and incubated again for 2 h at room temperature. Between each step, plates were washed using an automated plate washer (ELx50, Bio-Tek) and the PBS/0.1% Tween20 wash buffer provided. One hundred microlitres hydrogen peroxidase and chromogen substrate solution were then added for 20 min in the dark followed by 50 μL sulfuric acid stop solution. The cytokine concentration in each well was then analysed using the plate reader (ELX800, Bio-Tek) at an optical density of 450 nm and 570 nm, with latter values subtracted from the former to eliminate optical imperfections. The resulting outputs were then calibrated against a standard curve to determine concentration and IL-1β, with percentage recovery (%) calculated by comparing concentrations expressed in test samples with those of positive controls. Pilot investigations revealed that the above-mentioned buffer solutions did not interfere with the assay (data not shown).

In vivo cross-sectional study

Setting

A cross-sectional study was conducted on the undergraduate endodontic specialty teaching clinics at Birmingham Dental Hospital between September 2021 and June 2022. All procedures were performed under a dental operating microscope (Global Surgical Corp.), by the lead investigator (SSV).

Participants

Medically fit consenting adults (≥18 years) undergoing root canal treatment in mature permanent teeth diagnosed with NAT or AAP were consecutively recruited. The exclusion criteria consisted of those who had undergone antimicrobial therapy 3 months prior to screening or were immunocompromised. Teeth with previously initiated endodontic treatment or existing root fillings; periodontal pocketing ≥5 mm; that were unable to retain a rubber dam; had apices closely associated with the maxillary sinus; exhibited clinical or radiographic signs of a periradicular abscess or cyst (i.e. ≥10 mm or corticated radiolucencies), root resorption or fracture were also excluded, alongside whole PTF samples where paper points were contaminated with profuse apical bleeding.

Sample size

Statistical methods for determining sample size could not be performed due to lack of prior data. Therefore, researchers collected as many samples as possible during the nine-month study period with minimum of 12 per group, as reported by (Sette-Dias et al., 2016).

Diagnostic reference standard

Diagnoses were made by two independent staff with postgraduate endodontic qualifications. Teeth were subjected to clinical (percussion and palpation) and plain-film radiographic examination in conjunction with thermal (Endo-Frost, Roeko) and electric pulp testing. Normal apical tissues were defined as teeth that clinically were not sensitive to percussion or palpation testing and radiographically exhibited an intact laminar dura with uniform periodontal ligament space. Conversely, AAP was defined as teeth that were also clinically not sensitive to percussion or palpation testing but radiographically demonstrated a periradicular radiolucency (Glickman, 2009).

Clinical protocol

Upon attaining local anaesthesia with 2% lidocaine and 1:80 000 adrenaline solution (Dentsply Sirona), teeth were isolated using rubber and liquid dam (Liquidam, Cerkamed). A traditional stable four-walled access cavity to the pulp chamber was then created with cooled diamond burs under high-volume aspiration. After gently washing and air drying away gross dentinal debris and residual moisture with a triple air syringe, a 10/0.02 K-Flex file (Dentsply Sirona) was advanced slowly down the canal whilst connected to a Dentaport ZX electronic apex locator (Morita). Initially, patency was confirmed when only the first red display bar became visible, after which files were retracted to the zero- (i.e. terminal green display bar) and 0.5-reading markers (i.e. fifth green display bar) to determine positions of the apical foramen and constriction, respectively (Connert et al., 2018). All sampling protocols were respective to the former whereas the latter was considered the working length for subsequent root canal preparation and obturation procedures. To improve accuracy, this process was repeated with a 15/0.02 alongside a periapical radiograph taken at the zero-reading via a paralleling technique (ESE, 2006). When file tips were ≥2 mm from the radiographic apex or extruded, length modifications were informed by a third electronic apex locator reading. Canals were then pre-flared by watch-winding a 20/0.02 file to the zero-reading in a crown-down manner, which also standardized the apical constrictions' diameter; dried using 25/0.02 paper points set 2 mm short of this measurement; and patency filed with a 10/0.02 to disrupt dentinal debris at the apices and encourage intraradicular influx of tissue fluid.

PTF sampling

Prior to any irrigation, PTF samples were collected with three paper points per tooth using an optimized protocol determined *in vitro*. Briefly, each cone was gripped with locking college tweezers at the length equating to the zero-reading plus the optimal insertion depth. It was then slowly advanced into the pre-flared canal until reaching this measurement, where the tweezers were unclasped and a digital countdown timer initiated. The exact parameters including brand, insertion depth relative to the zero-reading, ISO size and sampling duration are outlined in the 'volume absorbance' subheading of the results section. If any of the three cones became contaminated by profuse apical bleeding, the entire sample was abandoned. Nevertheless, once sampled, cones were immediately transferred into sterile microfuge tubes, normalized according to total fluid volume (TFV) in 250 μL of sterile buffer solution, eluted using optimized parameters determined *in vitro* and stored at -80°C until analysis. The exact eluting buffer and technique used can be found in the 'analyte recovery' subheading of the results section. In posterior teeth, samples were retrieved from maxillary palatal and mandibular distal root canals.

PTF analyses

Wetted lengths (mm) of paper points were measured immediately after sampling and calibrated as per *in vitro* methods to calculate total absorbed PTF volume (μL) per sample.

The Bradford dye-binding assay (Thermo Fisher Scientific) was performed to determine the total protein concentration (TPC; μg/mL). Briefly, 5 μL of standards and samples were added to a clear flat bottom 96-well plate in duplicates followed by 250 μL of Bradford reagent. Plates were incubated for 20 min at room temperature with the optical density determined using a plate reader at 595 nm (Tecan Spark). Values were subtracted from those attained from a negative control (i.e. buffer solution only). The TPC was then calculated against a standard series of BSA.

The Target-48 Panel (O-link) was used to quantify the concentration (pg/mL) of 45 different proteins within each sample. Briefly, 1 μL of samples, standards and controls were transferred into a 96 well polymerase chain reaction (PCR) plate and incubated overnight at 4°C with 3 μL of incubation mix consisting of protein binding antibody pairs alongside conjugated DNA tags. Thereafter, the unique DNA reporting sequences generated were amplified for each target protein by adding 96 μL of extension mix to wells and a PCR thermocycler. Thereafter, 2.8 μL extension PCR products and 7.2 μL of detection mix was added to a new 96-well PCR plate, with the DNA reported for each target protein being quantified via high-throughput microfluidics real-time quantitative PCR. All outputs were normalized to TFV and presented as pg/TFV (Mente et al., 2016). Cytokines were considered absent, and excluded from analyses, when concentrations fell below the lower limit of detection in >25% of test PTF samples. Data points were assigned zero and maximum values when readings were below or above the respective limits of detection. All assays were performed in duplicates as per manufacturer's instructions.

Statistical analyses and data presentation

All data were coded by SSV for assessor blinding and statistically analysed per protocol in 'R' (V.4.1.0) software by NZB. Descriptive statistics were presented as medians with [interquartile range] in dot plots using GraphPad Prism software (V.8.0.2). For group comparisons, normality screening was conducted using the Shapiro-Wilks test. Normally distributed groups were compared using one- and two-way ANOVAs with *post hoc* Bonferonni correction tests and skewed groups with Mann–Whitney *U* tests. Independent-samples *t*- and chi-squared tests were used to compare baseline characteristics between groups. Initial alpha values for the *in vitro* and *in vivo* studies were set at .05 and .01, respectively.

Principal component analysis (PCA) was performed to identify clusters of analytes highly associated with AAP. Briefly, Target-48 data was dimensionally reduced into linear variables termed principal components (PC) with those possessing eigenvalues >1 included in further analyses. Loadings were computed against PCs to determine correlations, which were visualized in PC biplots. These were supplemented with a seriated heat map and network analysis graphs depicting only significant ($p < .05$) interactions ($r > .75$) using Gephi (V.0.9.7) software.

Diagnostic performance was determined using receiver operator characteristic (ROC) curves and presented as area under the curve (AUC) with [95% confidence intervals (95%CI)]. Diagnostic accuracy was then classified according to criteria outlined by Šimundić (2009). For individual analytes, optimal cut-offs, and sensitivity and specificity at that concentration, were identified by maximizing the Youden's *J* Index ([sensitivity + specificity] -1; Youden, 1950). For the PCA-derived cluster, continuous data for each constituent peptide was dichotomised using the respective diagnostic thresholds and subsequently entered into a multivariable logistic regression model to calculate AUC. All ROC curves were generated using a leave-one-out cross-validation (LOOCV) approach (Grant et al., 2022).

RESULTS

Results are summarized in Tables 1 and 2 and Figure 2 for the *in vitro* studies and Tables 3 and 4 and Figures 3–6 for the *in vivo* study. Raw data supporting the findings of this study are available from the corresponding author upon reasonable request.

In vitro methodological studies

Volume absorbance

Classic (UnoDent) was the most absorbent brand of paper point ($p < .05$), with no significant differences occurring after 60 s (1.6 μL [1.30–1.73]), 1 mm insertion depth, which would be relative to the EAL's zero-reading (1.6 μL [1.43–1.71]), and up to a size 40/0.02 (2.2 μL [1.98–2.20]).

Analyte recovery

IL-1β recovery ranged from 67.6% to 98.3% with significant differences amongst eluting buffers and techniques ($p < .05$). Overall yields were highest following vortexing (89.3% [82.28–96.41]) and PBS/1%BSA buffer (86.9% [81.44–110.47]) and lowest following incubation, vortexing and centrifugation (80.3% [75.05–84.95]) and PBS (79.9% [73.48–86.80]).

In vivo cross-sectional study

Participant characteristics

Fifty-two PTF samples (NAT: 19; AAP: 33) were retrieved after screening 71 individuals; however, only 44 (NAT: 13; AAP: 31) proceeded to analysis due to profuse apical bleeding. The median patient age was 44 [29–55] (NAT: 63 [46–67]; AAP: 37 [28–51]) with an approximate 1:1 male-to-female ratio. Three participants (NAT: 1; AAP: 2) were of Afro-Caribbean descent, 7 were Asian (NAT: 2; AAP: 5) and 34 were Caucasian (NAT: 10; AAP: 24). Eighteen (NAT: 6; AAP: 12) samples were collected from mandibles and 26 (NAT: 7; AAP: 19) maxilla with incisors/canines being the commonest tooth (18; NAT: 2; AAP: 16) followed by molars (14; NAT: 4; AAP: 10) and premolars (12; NAT: 7; AAP: 5). Groups were matched by gender, ethnicity and interarch tooth position.

PTF characteristics

Wetted lengths were significantly greater in AAP samples ($p < .001$). This translated into larger PTF volumes (1.7 μL [0.70–2.59]) when compared with the NAT group (0.2 μL [0.10–1.53]; $p < .01$). Additionally, AAP samples exhibited 249.0 μg/mL [63.25–373.42] TPC as opposed to 3.8 μg/mL [0–13.75] in controls ($p < .01$).

TABLE 1 Optimizing parameters for maximum paper point absorbance (μL) following *in vitro* PTF sampling.

Parameter	Absorbed volume (μL)			
Paper point brand	**Classic***	**DeTrey**	**DiaDent**	**HS Maxima**
	1.6 [1.30–1.73]	0.6 [0.40–0.80]	0.7 [0.58–0.83]	0.9 [0.70–1.10]
	Kerr	**Maillefer**	**Orbis**	**Panadent**
	0.9 [0.64–0.10]	0.7 [0.45–0.83]	0.9 [0.60–1.23]	1.0 [0.80–1.30]
	QED DiaDent	**Roeka Colour**	**SybronEndo**	**VDW**
	0.6 [0.40–0.63]	0.7 [0.58–0.90]	1.1 [0.80–1.53]	0.5 [0.40–0.70]
Paper point size (ISO)	**15/0.02**	**20/0.02**	**25/0.02**	**30/0.02**
	1.6 [1.30–1.73]	1.6 [1.30–1.90]	1.9 [1.55–2.25]	1.9 [1.68–2.43]
	35/0.02	**40/0.02**[a,b]		
	1.7 [1.40–2.25]	2.2 [1.98–2.20]		
Sampling duration (s)	**30***	**60**	**90**	**120**
	0.7 [0.60–0.83]	1.5 [1.30–1.73]	1.5 [1.30–1.73]	1.6 [1.50–1.73]
	150	180		
	1.5 [1.30–1.70]	1.6 [1.35–1.90]		
Insertion depth (mm)	**1**	**2**	**3**	**4**
	1.6 [1.30–1.73]	1.6 [1.38–1.80]	1.4 [1.20–1.63]	1.4 [1.40–1.63]

Note: Results for each group ($n = 20$) presented as medians and [interquartile ranges]. [*] versus all other groups; [a] versus ISO # 15; [b] versus ISO # 20 ($p < .05$ – One-way ANOVA and *post-hoc* Bonferroni test).

TABLE 2 Optimizing parameters for maximum analyte recovery (%) following *in vitro* PTF elution.

	IL-1β recovery (%)				
Buffer	**Vortex[a]**	**Vortex, centrifuge[b]**	**Centrifuge[c]**	**Incubate, vortex, centrifuge[d]**	**Overall Buffer**
PBS[i]	74.7[b–d] [70.24–78.06]	76.9[b,c] [74.20–80.94]	81.0 [80.66–83.81]	79.2 [73.48–82.91]	79.9[b,c] [73.62–86.80]
PBS & BSA[ii]	94.1[a,iii] [87.74–100.44]	98.3[a,d,iii,iv] [88.74–106.70]	81.8[i,ii] [80.40–83.79]	86.1[ii] [81.57–86.68]	86.9[a,d] [81.44–110.47]
PBS & Tween20[iii]	95.4[a,iv] [93.72–97.27]	94.9[a,d,iii,iv] [92.85–96.91]	84.0[i] [80.92–84.54]	73.7[i,ii] [72.95–77.42]	85.5[a,d] [79.52–104.17]
PBS & NaCl[iv]	92.5[a,ii,iii] [86.81–95.42]	67.6[b,c,i,iv] [59.27–77.70]	80.0[i] [73.17–84.69]	84.5[ii] [79.27–85.12]	83.9[b,c] [74.34–99.98]
Overall Technique	89.3[iii,iv] [82.28–96.41]	84.9 [74.48–94.7]	81.8[i] [80.00–84.65]	80.5[i] [75.05–84.95]	

Note: Results for each group ($n = 6$) presented as medians and [interquartile ranges]. [[a]] versus corresponding PBS; [[b]] versus corresponding PBS and BSA; [[c]] versus corresponding PBS and Tween20; [[d]] versus corresponding PBS and NaCl; [[i]] versus corresponding vortex; [[ii]] versus corresponding vortex and centrifuge; [[iii]] versus corresponding centrifuge; [[iv]] versus corresponding incubate, vortex and centrifuge ($p < .05$ – Two-way ANOVA and *post hoc* Bonferroni test).

Abbreviations: BSA, bovine serum albumin; NaCl, sodium chloride; PBS, phosphate-buffered saline; IL-1β, interleukin 1 beta.

Proteomic analysis

The Target-48 panel consistently detected 18, of a potential 45, analytes. These included Chemokine Ligand [CCL]-2, -3 and -4; Colony Stimulating Factor [CSF]-1; Chemokine Ligand [CXCL]-9; Hepatocyte Growth Factor [HGF]; Interleukin [IL]-1β, -6, -8 [CXCL-8], -17A and -18; MMP-1 and -12; Oxidized Low Density Lipoprotein Receptor [OLR]-1; Oncostatin M [OSM]; Tumour Necrosis Factor Superfamily [TNFSF]-10 and 12 and Vascular Endothelial Growth Factor [VEGF]-A. Concentrations were significantly greater ($p < .001$) in AAP samples, with the most abundant cytokines detected being ORL-1 (567.4 pg/TFV [257.98–874.21]), MMP-12 (264.5 pg/TFV [107.80–1314.25]), CXCL-8 (206.8 pg/TFV [54.18–760.58]) and IL-1β (92.6 pg/TFV [23.24–211.80]). The 27 less frequently detected analytes are detailed in Appendix S1.

Correlations with disease state

The first three PCs, representing 61.6%, 8.5% and 6.3% variance, respectively, were included in PCA. Loadings revealed PC1 to be positively correlated to AAP with higher expressions of all 18 analytes. The second PC exhibited minimal correlations with AAP, lower expression of CCL-3, -4, IL-1β, -6, -17A, -18 and higher expressions of MMP-12, TNFSF-10, VEGF-A. PC3 was negatively correlated with AAP with downregulation of CXCL-8, IL-1β, OLR-1 and upregulation of CXCL-9, IL-6, -17A, MMP-1. The PC biplots and seriated heat maps identified strong positive correlations between AAP and an analyte cluster consisting of CXCL-8, IL-1β, OLR-1, OSM, TNFSF-12. Network analysis graphs illustrate that analyte composition and number of associations are substantially greater and more complex in diseased tissues. Only 13 analytes formed the NAT network with exclusions of CSF-1, CXCL-9, IL-17A, TNFSF-10, -12. Conversely, all 18 cytokines formed the AAP network and contributed to a greater abundance. Heat maps revealed positive associations between all analytes.

Diagnostic performance

Individually, TNFSF-12 exhibited the highest diagnostic performance (AUC: 0.94 [0.86–1.00]) and sensitivity (1.00 [1.00–1.00]) and specificity (0.87 [0.77–0.97]) at its diagnostic threshold (0.90 pg/TFV). It was thus considered an 'Excellent' (AUC: >0.9–1.0) discriminator between AAP and NATs. The remaining analytes were deemed 'Very Good' (AUC: >0.8–0.9; HGF, IL-17A, MMP-1, OLR-1, TNFSF-10, VEGF-A), 'Good' (AUC: >0.7–0.8; CCL-3, −4, CSF-1, IL-18, MMP-12, OSM), 'Sufficient' (AUC: >0.6–0.7; CCL-2, IL-1β, IL-6, CXCL-8) or 'Bad' (AUC: >0.5–0.6; CXCL-9). With exception to TNFSF-12, they all generally exhibited higher sensitivity (0.87–0.1) than specificity (0.55–0.8) at their respective cut-offs. The PCA-derived cluster, however, increased diagnostic accuracy and precision (AUC: 0.96 [0.89–1.00]). Supplementary diagnostic performance data is detailed in Appendix S2.

DISCUSSION

The *in vitro* studies investigated several basic parameters associated with PTF sampling. Unodent's 'Classic' 15/0.02

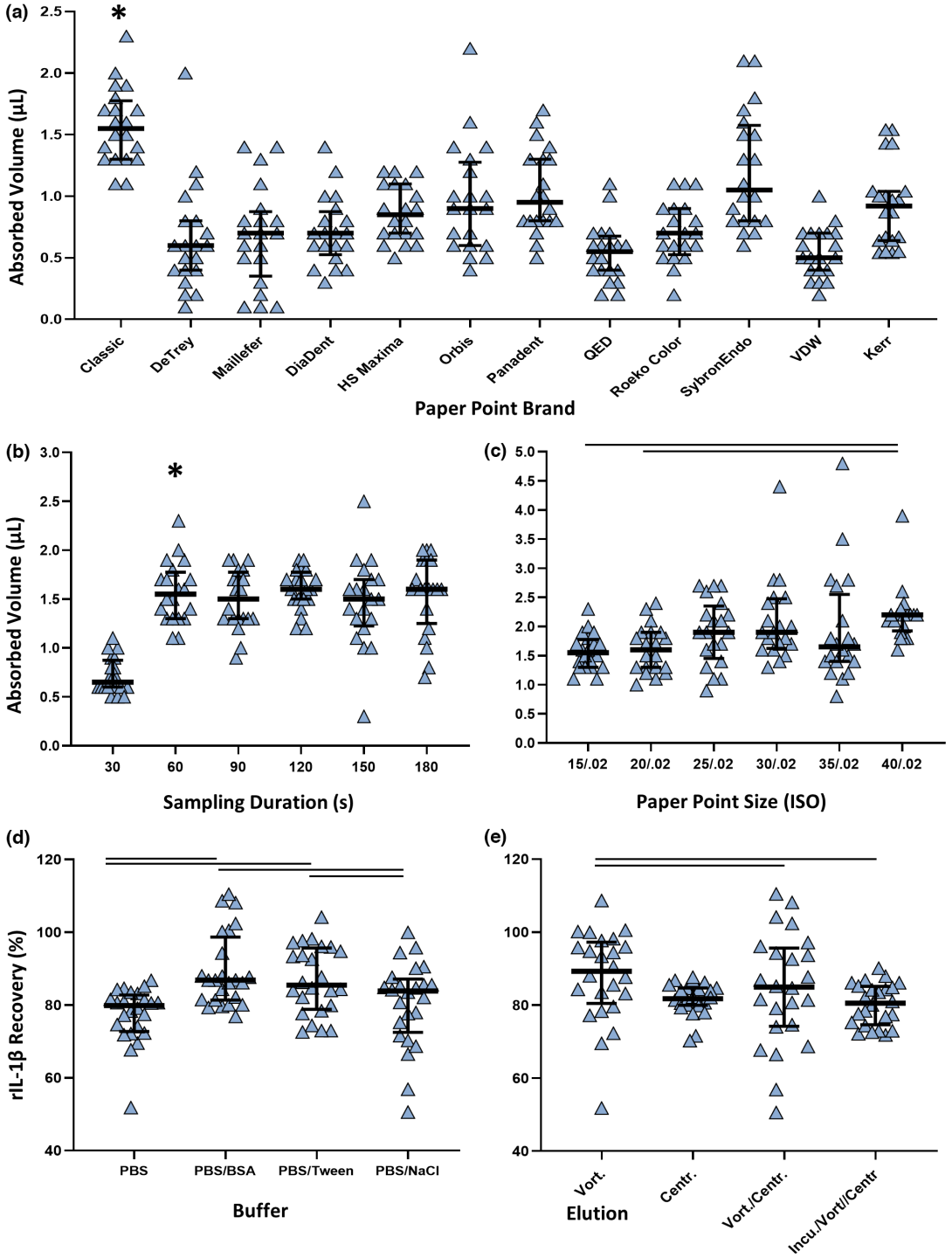

FIGURE 2 *In vitro* optimization of PTF during the sampling ($n = 20$) and eluting process ($n = 6$). Mock PTF absorbed volume (µL) with different: (a) brands of paper points; (b) sampling duration and (c) ISO size. Percentage recovery (%) of IL-1β following use of various (d) buffers and (e) eluting techniques. Data presented as dot plots where central bars represent the median alongside interquartile range for whiskers. Significant differences ($p < .05$; one- and two-way ANOVAs with *post hoc* Bonferroni tests) represented by [horizontal lines] = versus individual groups; [*] = versus all corresponding groups. BSA, bovine serum albumin; IL-1β, interleukin 1 beta; NaCl, sodium chloride; PBS, phosphate-buffered saline.

paper points inserted for 60 s at 1 mm depth relative to the zero-reading, followed by 60 s vortexing into 250 µL PBS/1% BSA facilitated the largest volume absorbance and IL-1β recovery, respectively. When applied clinically to identify potential biomarkers of endodontic disease, AAP samples had greater paper point wetted length, absorbed volume and TPC than their NAT counterparts. Proteomic analysis consistently identified 18 peptides, all

TABLE 3 Baseline characteristics for samples of PTF.

Sample characteristics		Diagnosis [*n* (%)]			
		Total (*n* = 44)	NAT (*n* = 13)	AAP (*n* = 31)	*p* Value
Age (years)	Median [IQR]	44 [29–55]	63 [46–67]	37 [28–51]	<.05[a]
Sex	Female	22 (50.0)	7 (53.8)	15 (46.9)	>.05[b]
	Male	22 (50.0)	6 (46.2)	16 (53.1)	
Ethnicity	Afro-Caribbean	3 (6.8)	1 (7.7)	2 (6.4)	<.05[b]
	Asian	7 (16.0)	2 (15.4)	5 (16.1)	
	Caucasian	34 (77.2)	10 (76.9)	24 (77.5)	
Inter-arch position	Mandible	18 (40.9)	6 (46.2)	12 (38.7)	>.05[b]
	Maxilla	26 (59.1)	7 (53.8)	19 (61.3)	
Intra-arch position	Incisor/Canine	18 (40.9)	2 (15.4)	16 (51.6)	<.05[b]
	Premolar	12 (27.3)	7 (53.9)	5 (16.1)	
	Molar	14 (31.8)	4 (30.7)	10 (32.3)	

[a]Independent-samples *t*-test.

[b]Chi-squared test.

Abbreviations: AAP, asymptomatic apical periodontitis; NAT, normal apical tissues.

of which were highly expressed in disease and associated with AAP, particularly CXCL-8, IL-1β, OLR-1, OSM and TNFSF-12. Whilst the latter individually demonstrated excellent diagnostic accuracy, the overall PCA cluster exhibited the highest discriminatory power and thus may serve as a reliable biosignature for AAP. All null hypotheses were, therefore, rejected.

In vitro methodological studies

There are several limitations associated with the present *in vitro* experiments. The volume absorbance model for instance lacks biofidelity, as it does not take into account surface tensions generated by root canal walls (Karamifar et al., 2012). This would influence fluid movement and could explain the extreme wetted length values observed *in vivo*. Further support for this phenomenon is derived from a pilot investigation into volume absorbance that utilized an extracted tooth model. When the tips of paper points were inserted into buffer solution via the pre-flared canal of a central incisor, capillary action was consistently observed which oversaturated the cone. As this gave a false representation of paper point absorbance capacity under various parameters, the approach was abandoned, Digital scales would have also been more precise determinants of volume absorbance as opposed to wetted length, which is subject to human measurements of uneven paper point saturation. It was, however, not adopted as both methods have been previously correlated to each other and balances accurate to 1 nanogram are not readily accessible in the clinical environment (da Cunha et al., 2008). For the eluting experiment, IL-1β was the only cytokine used to determine the effectiveness of several extraction buffers and techniques. Caution should, therefore, be taken when extrapolating these recovery rates to other analytes (Inic-Kanada et al., 2012).

Classic (Unodent) was identified to be the most absorbent paper point brand. This could be attributed to larger pore sizes within its cellulose membrane (Zehnder et al., 2014), which may also explain their less ridged and fibre-shedding properties (Brown, 2017). Surprisingly, no meaningful volume could be further attained after 60 s sampling duration, a curvilinear relationship also observed by Shimauchi et al. (1996), and a 1 mm insertion depth. The latter would be advantageous *in vivo* as there would be less risk of cellulose fibres shedding into the periradicular tissues and inducing a persistent foreign body reaction (Nair, 2004). Whilst 40/0.02 s were significantly more absorbent, they were impractical for *in vivo* application as they could not pass through apical constrictions without erroneous enlargement. Instead, 15/0.02 s were selected as they demonstrated as much absorbency as 35/0.02 s whilst also conforming to the physiological diameter of the minor apical foramen (Chapman, 1969; Dummer et al., 1984). For IL-1β elution, retrieval rates were consistent with those reported by Inic-Kanada et al. (2012), but higher than those found by Shimauchi et al. (1996; 56%–67%). Methodological differences such as more porous paper point material, which has been proposed to lead to less physical entrapment of cytokines (Inic-Kanada et al., 2012), and larger initial loading doses may explain these discrepancies. Nevertheless, when the overall buffer effectiveness was considered, PBS achieved the lowest yields whereas the remaining solutions were relatively interchangeable. These findings are consistent

TABLE 4 Analysis of PTF collected from *in vivo* sampling.

	Diagnosis		PC loadings			Diagnostic performance [95% CI]			
PTF characteristics	**NAT ($n=13$)**	**AAP ($n=31$)**	**PC1**	**PC2**	**PC3**	**AUC**	**Cut-off**	**Sensitivity**	**Specificity**
Total absorbed volume (μL)	0.2 [0.10–1.53]	1.7 [0.70–2.59]*							
Total protein concentration (μg/mL)	3.8 [0–13.75]	249.0 [63.25–373.42]*							
Analyte concentration (pg/TFV)									
Chemokine ligand [CCL]-2	0.1 [0.06–0.96]	7.8 [1.87–26.10]*	0.21	0.02	0.15	0.69 [0.56–0.83]	1.12	0.87 [0.77–0.83]	0.69 [0.56–0.83]
Chemokine ligand [CCL]-3	0.2 [0.06–0.61]	7.4 [1.74–21.15]*	0.25	−0.32	0.05	0.80 [0.69–0.92]	1.13	0.93 [0.85–1.00]	0.69 [0.55–0.82]
Chemokine ligand [CCL]-4	0.8 [0.055–1.67]	25.5 [8.35–68.10]*	0.26	−0.20	0.12	0.74 [0.62–0.87]	4.38	0.92 [0.84–1.00]	0.58 [0.43–0.72]
Colony stimulating factor [CSF]-1	0.1 [0.06–0.18]	1.3 [0.59–3.12]*	0.28	0.10	0.02	0.80 [0.69–0.92]	0.34	0.93 [0.85–1.00]	0.69 [0.55–0.82]
Chemokine ligand [CXCL]-9	1.0 [0.57–1.37]	2.7 [0.36–5.78]*	0.16	0.17	0.34	0.60 [0.46–0.75]	0.10	0.92 [0.84–1.00]	0.55 [0.40–0.70]
Hepatocyte growth factor [HGF]	0.8 [0.31–1.54]	57.4 [27.73–113.93]*	0.28	0.09	0.07	0.86 [0.76–0.96]	5.56	0.96 [0.91–1.00]	0.75 [0.62–0.88]
Interleukin [IL]-1β	0.9 [0.16–2.17]	92.6 [23.24–211.80]*	0.18	−0.31	0.23	0.69 [0.54–0.83]	10.03	0.93 [0.85–1.00]	0.69 [0.55–0.82]
Interleukin [IL]-6	0.3 [0.028–0.63]	3.2 [0.88–9.69]*	0.24	−0.25	−0.05	0.68 [0.56–0.83]	1.14	0.95 [0.89–1.00]	0.55 [0.40–0.69]
Interleukin [CXCL]-8	4.6 [0.28–40.85]	206.8 [54.18–760.58]*	0.24	0.05	−0.33	0.68 [0.54–0.82]	200.17	0.91 [0.82–0.99]	0.50 [0.35–0.65]
Interleukin [IL]-17A	0.1 ± [0.08–0.12]	0.8 [0.41–2.78]*	0.19	−0.19	−0.50	0.84 [0.73–0.95]	0.23	1.00 [1.00–1.00]	0.68 [0.55–0.82]
Interleukin [IL]-18	0.4 [0.26–1.11]	46.6 [28.32–93.75]*	0.16	−0.44	0.22	0.79 [0.67–0.91]	4.05	0.93 [0.86–1.00]	0.79 [0.66–0.91]
Matrix metallopeptidase [MMP]-1	0.2 [0.034–0.837]	58.2 [12.19–177.26]*	0.22	−0.06	0.31	0.87 [0.77–0.97]	2.02	1.00 [1.00–1.00]	0.76 [0.64–0.89]
Matrix metallopeptidase [MMP]-12	0.3 [0.11–6.18]	264.5 [107.80–1314.25]*	0.20	0.50	0.16	0.74 [0.62–0.87]	37.98	0.88 [0.79–0.98]	0.56 [0.41–0.70]
Oxidized low density lipoprotein receptor [OLR]-1	13.6 [2.36–36.44]	567.4 [257.98–874.21]*	0.25	0.08	−0.24	0.83 [0.72–0.94]	91.76	0.97 [0.91–1.00]	0.80 [0.68–0.92]
Oncostatin M [OSM]	0.7 [0.17–1.62]	14.5 [4.01–37.87]*	0.24	−0.09	−0.12	0.74 [0.61–0.87]	3.88	1.00 [1.00–1.00]	0.62 [0.48–0.76]
Tumour necrosis factor superfamily [TNFSF]-10	2.1 [1.69–2.60]	18.3 [7.16–46.38]*	0.26	0.28	0.02	0.87 [0.77–0.97]	3.54	0.93 [0.85–1.00]	0.69 [0.55–0.82]
Tumour necrosis factor superfamily [TNFSF]-12	0.6 [0.40–0.75]	12.5 [5.18–26.55]*	0.25	0.12	−0.07	0.94 [0.86–1.00]	0.90	1.00 [1.00–1.00]	0.87 [0.77–0.97]
Vascular endothelial growth factor [VEGF]-A	2.1 [0.35–4.35]	47.3 [23.79–93.37]*	0.27	0.25	0.06	0.83 [0.72–0.94]	8.37	0.97 [0.91–1.00]	0.80 [0.68–0.92]
Presence of AAP	—	—	0.16	0.03	−0.41	—	—	—	—
PCA cluster (CXCL—8; IL-1β; OLR-1; OSM; TNFSF-12)	—	—	—	—	—	0.96 [0.89–1.00]	—	1.00 [1.00–1.00]	0.87 [0.77–0.97]

Note: Results presented as median and [interquartile range].

Abbreviations: 95% CI, confidence interval; AAP, asymptomatic apical periodontitis; AUC, area under curve; NAT, normal apical tissues; PC, principal component; PCA, principal component analysis; ROC, receiver operator characteristic; TFV, total fluid volume.

*$p < .01$ Mann–Whitney *U* test.

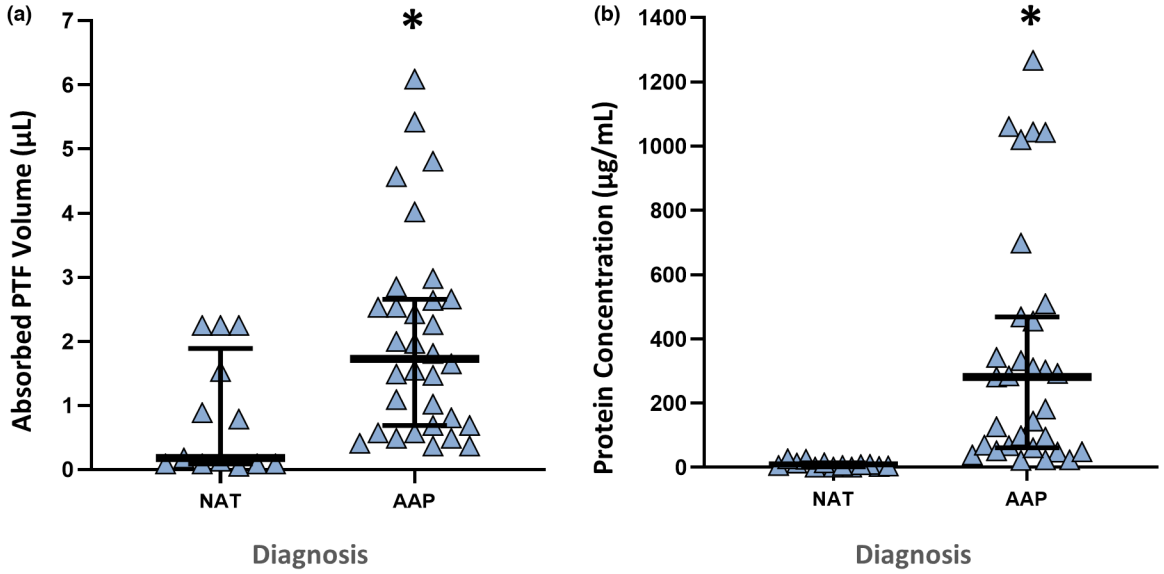

FIGURE 3 Characteristic of PTF following *in vivo* sampling. (a) absorbed PTF volume (µL); (b) total protein concentration (µg/mL). Data presented as dot plots where central bars represent the median alongside interquartile range for whiskers. Significant differences ($p < .05$; Mann–Whitney *U* tests) represented by [*]. AAP, asymptomatic apical periodontitis ($n = 31$); NAT, normal apical tissues ($n = 13$); PTF, periradicular tissue fluid.

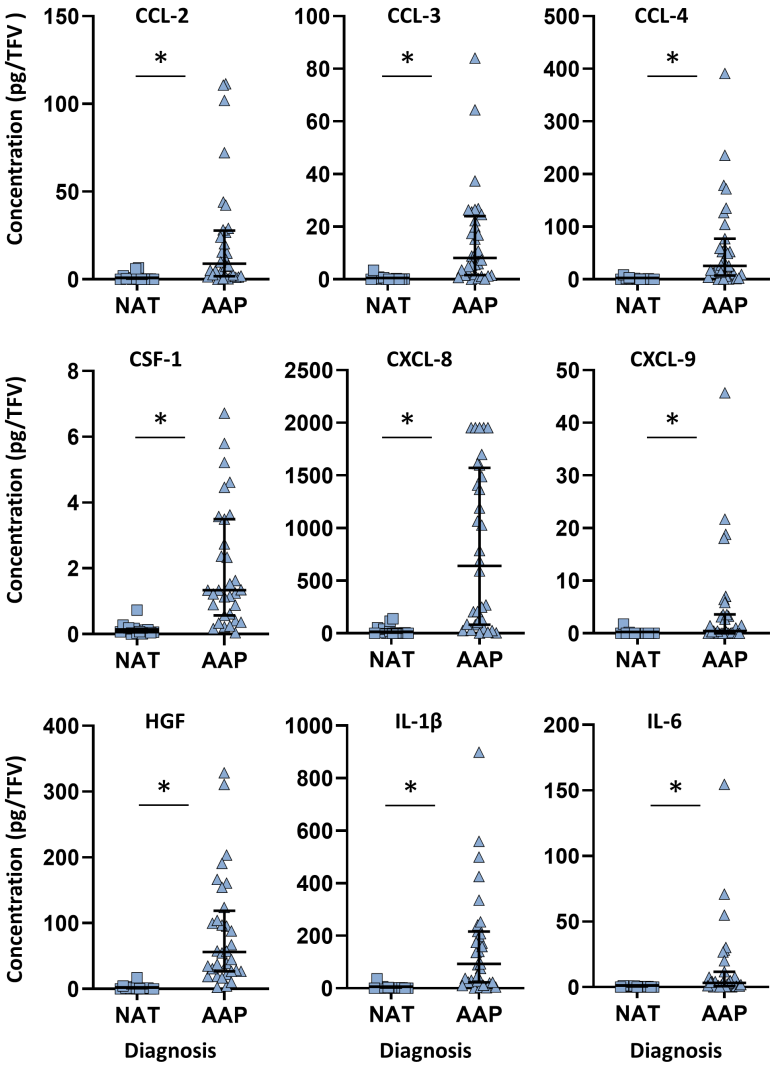

FIGURE 4 Concentration (pg/TFV) of analytes detected within PTF following *in vivo* sampling. Data presented as dot plots where central bars represent the median alongside interquartile range for whiskers. Significant differences ($p < .001$; Mann–Whitney *U* tests) represented by [*]. AAP, asymptomatic apical periodontitis ($n = 31$); NAT, normal apical tissues ($n = 13$). CCL-2, chemokine ligand-2; CCL-3, chemokine ligand-3; CCL-4, chemokine ligand-4; CSF-1, colony stimulating factor-1; CXCL-8, interleukin/chemokine ligand-8; CXCL-9, chemokine ligand-9; HGF, hepatocyte growth factor; IL-17A, interleukin-17A; IL-18, interleukin-18; IL-1β, interleukin-1β; IL-6, interleukin-6; MMP-1, matrix metallopeptidase-1; MMP-12, matrix metallopeptidase-12; OLR-1, oxidized low density lipoprotein receptor-1; OSM, oncostatin M; TNFSF-10, tumour necrosis factor superfamily-10; TNFSF-12, tumour necrosis factor superfamily-12; VEGF-A, vascular endothelial growth factor-A.

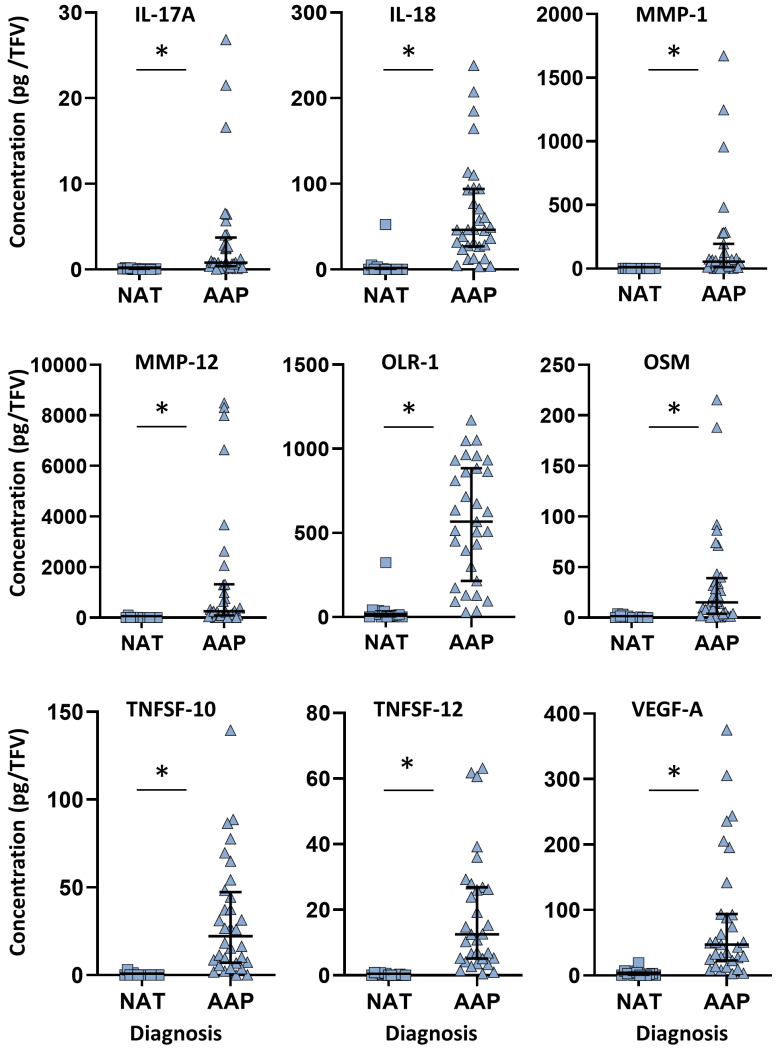

FIGURE 4 (Continued)

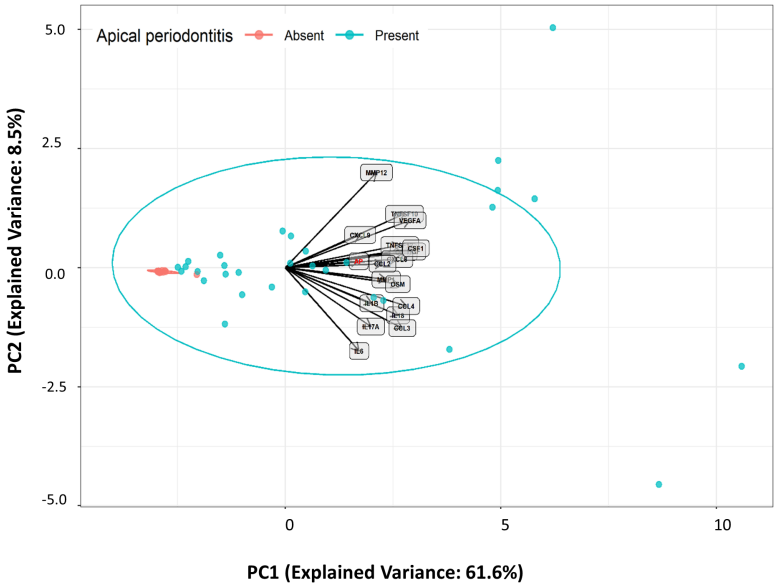

FIGURE 5 Principal component analysis evaluating the correlation of various analytes to each other and disease states. PC1 versus PC2 biplot.

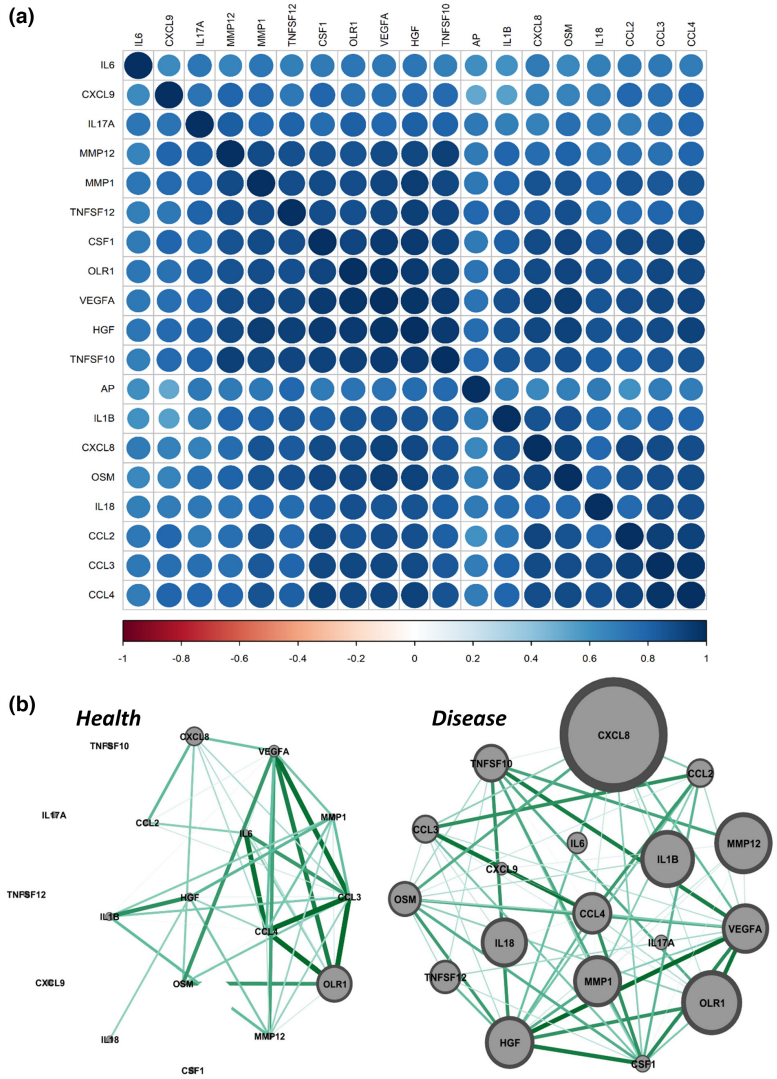

FIGURE 6 Heat map and network analysis graphs. (a) Seriated heat map demonstrating positive (blue) and negative (orange) correlations between analytes and presence of asymptomatic apical periodontitis. Variables plotted closer together were more similar. (b) Network analysis graphs demonstrating positive (green) and negative (red) correlations between analytes relative to disease state. Cytokines and significant correlations ($r > .75$; $p < .05$) were represented as nodes and connections, respectively. Node size was relative to the median concentration of analytes, and their degree of connectivity, with stronger associations depicted as darker and wider connections.

with the favourable properties of BSA, Tween20 and NaCl in that they preserve macromolecular integrity and reduce nonspecific protein binding (Mao et al., 2007; Steinitz, 2000). With respect to eluting techniques, vortexing alone revealed the greatest percentage of recovery. The high velocities of oscillating forces generated may thus be more suited to shedding proteins entrapped in the paper point meshwork or bound to plastic column walls than centrifugal forces (Zhou et al., 2006).

In vivo cross-sectional study

The Target-48 panel was selected due to several advantages over other arrays. Only 1 μL of sample was required to simultaneously quantify 45 cytokines, the proximity extension technology offered exceptionally high sensitivity and specificity and prior q-values demonstrate low false positive rates of analyte detection (Katz et al., 2022; Wik et al., 2021). Furthermore, pilot investigations confirmed that the eluting buffer or exudate matrix did not interfere with internal assay controls, as was observed with other immunoassays.

The present results nevertheless, still need to be interpreted with caution due to several methodological limitations. Most notably, it was not possible to normalize crude analyte values to TPC due to low yields found in NATs, an issue similarly observed by Zehnder et al. (2014) in dentinal tubular fluid. Normalizing to TFV, an alternative strategy utilized in several prior investigations (Ballal et al., 2017; Mente et al., 2016; Teixeira et al., 2022; Wahlgren et al., 2002;

Zehnder & Belibasakis, 2022) and suggested by Zehnder and Belibasakis (2022), may thus be necessary when comparing transudates to exudates. This approach, however, increases risk of type 1 errors as differences in analyte concentration may be overestimated, which is why initial alpha values were set to 0.01. The apical constrictions physiological diameter may also limit the volume of PTF that can enter into the canal and thus, be absorbed. Whilst teeth with a minor apical foramen width of ≤0.2 mm will have been standardized via the above protocol (Chapman, 1969), those naturally larger than this may, therefore, have introduced a sample bias. This could have contributed to the substantial variations observed in total absorbed volume. Attempting to standardize to diameters larger than this, however, may inadvertently introduce noxious insults to the periradicular tissues during root canal preparation and obturation. Other limitations include a small sample size, uneven recruitment rate and several unmatched baseline characteristics; all of which introduce selection bias. Contributing factors include convenient sampling and difficulties in attaining PTF from healthy teeth, as they were less frequently encountered and more prone to profuse apical bleeding. Cytokines demonstrating only modest concentration increases (i.e. IL-6, -17A and CSF-1) or a broad spread of data (i.e. CXCL-8 and MMP-12) may, therefore, be underpowered and their significance should be interpreted with caution. This, however, will not be applicable to all mediators with many exhibited highly significant differences.

The objective reference gold standard for confirming endodontic diagnosis is histological examination. As this is not clinically applicable, the presence or absence of periradicular disease in the current study was based on clinical and radiographic signs and symptoms outlined in the American Association of Endodontist guidelines (Glickman 2009). It is acknowledged greater accuracy could have been achieved with cone-beam computed tomography (Patel et al., 2009); however, this facility was not readily accessible. Therefore, there may have been PTF samples obtained from diseased teeth perceived to have NATs and to a lesser extent, vice versa. This was, however, unlikely as most control samples were retrieved from teeth undergoing elective root canal treatment and only unambiguous radiographic lesions were included in the AAP group. Moreover, to improve generalizability of the diagnostic data, it would have been ideal to perform the current investigation in a similar but independent cohort across several sites as per Grant et al. (2022). The present funding could not permit this and so a LOOCV statistical method was used to reduce overlap between training and test data during performance analyses. Each sample would have, therefore, mimicked an externally validating observation, ultimately leading to more robust and less bias AUC values.

The *in vivo* study consistently identified 18 analytes in PTF samples from teeth with AAP. These comprised of chemokines (CCL2, -3, -4, CXCL-8, -9) cytokines (CSF-1, IL-1β, -6, -17A, -18, OSM, TNFSF-10, -12), growth factors (HGF, VEGF-A), enzymes (MMP-1, -12) and receptors (OLR-1), all of which are of macrophage and/or T cell origin (Marton & Kiss, 1993; Silva et al., 2007). Their detection is supported by numerous immunohistochemical investigations into periapical lesions that have previously identified 12 of these biomarkers (Hasegawa et al., 2021; Kabashima et al., 2001; Nonaka et al., 2008; Tsai et al., 2008; Weber et al., 2019). Interleukin-1β, -6, -8, -17A and MMP-1 specifically have already been quantified at comparable levels in PTF (Virdee et al., 2019), with this study being the first to report on the remaining 13. Amongst this panel were several analytes with little prior association with apical periodontitis, including the pro-angiogenic and -regenerative HGF (Grant et al., 1993); IL-18, a modulator of lymphocytic activity (Nakanishi et al., 2001); MMP-12, otherwise known as elastase; OLR-1, an up-regulator of osteoclastogenesis (Ohgi et al., 2018); and TNFSF-10 and -12, both of which induce apoptosis (Kataria et al., 2010). Interestingly, several well-established pro-inflammatory mediators, namely Tumour Necrosis Factor [TNF]-α and Interferon [IFN]-γ, were undetected. These data conflicts with prior PTF studies and the high concentrations of CXCL-9 and IL-18 observed in this investigation, as the former upregulates expressions of both whilst the latter stimulates IFN-γ production (Kwak et al., 2005; Martinho et al., 2015; Nakanishi et al., 2001; Pezelj-Ribarić et al., 2007). One explanation for this may be that these analytes are more active in acute, as opposed to quiescent, phases of apical disease (Ferreira et al., 2016; Rechenberg et al., 2014).

When data were analysed for correlations, CXCL-8, IL-1β, OLR-1, OSM and TNFSF-12 were found to be highly associated with the presence of AAP. PTF-derived IL-1β has previously been correlated to several clinical symptoms characteristic of periradicular disease (Ataoğlu et al., 2002; Matsuo et al., 1994; Shimauchi et al., 1998); whilst GCF studies reported similar relationships for the remaining molecules; with exception of OLR-1 for which there is limited literature (Majeed et al., 2016). Moreover, network analyses revealed the diseased state to be significantly more complex than health. Numerous connections were present for any individual mediator, suggesting a capacity for the periradicular inflammatory response to adapt and persist. This reflects the complexity of the periapical disease process, which is not yet fully understood, and makes it difficult to identify an individual analyte to therapeutically target. Notable correlations that add validity to the data were found between CCL-2, -3 and -4, all of which share similar receptors and have demonstrated

cross-functionality (Repeke et al., 2010); and HGF and VEGF-A, with the former known to upregulate expression of the latter during wound healing (Reisinger et al., 2003). Similar associations requiring further investigation include VEGF-A and TNFSF-10; VEGF-A and OLR-1; and HGF and CSF-1.

The present diagnostic analysis reveals PTF as being a valid source of biomarkers for distinguishing periradicular disease from health. This objective information would be clinically useful for confirming the resolution of periapical inflammation immediately prior to obturation, particularly considering treatment outcomes are currently determined via temporal analysis of plain-film radiographs (ESE, 2006). Specific clinical situations that would benefit include orthograde treatment of larger lesions where root end surgery may be anticipated or assisting diagnosis of nonspecific orofacial pain in patients with previously initiated root canal treatment. Generally, PTF-derived analytes independently exhibited excellent sensitivity, but it is acknowledged that they lacked the same levels of specificity thus clinically risking over treatment. This was, however, abated when a combination of consistently present biomarkers were used, as the PCA-derived cluster increased diagnostic accuracy and precision (AUC: 0.96 [95% CI: 0.89–1.00]). These observations were previously observed by Grant et al. (2022) for combinations of GCF-derived peptides and also conform to the recently published guidelines for biomarker analysis which promotes the notion of biosignatures (Zehnder & Belibasakis, 2022). Of note, when analytes were evaluated individually, TNFSF-12 possessed the most discriminatory power and so according to this study is considered the most reliable individual biomarker for AAP. This reflects other diagnostic reports for marginal periodontal and peri-implant diseases (Yakar et al., 2019). Further independent analyses, however, need to be conducted to externally validate this data.

CONCLUSION

This two-part study optimized PTF sampling protocols *in vitro* and applied them clinically, alongside a high-throughput panel, to characterize the proteome of healthy and inflamed periapical tissues. A complex interconnected network of 18 potential biomarkers were identified, with CXCL-8, IL-1β, OLR-1, OSM and TNFSF-12 being most associated with the presence of AAP. Both TNFSF-12 and this overall cluster exhibited an excellent diagnostic ability to discriminate periradicular disease from health. The latter could thus be considered a biosignature for AAP. Longitudinal investigations with larger sample sizes are warranted to validate findings and correlate these mediators with long-term treatment outcomes. Furthermore, cell culture experiments to determine the exact roles of OLR-1, OSM, TNFSF-10 and -12 in periradicular pathophysiology are also required.

AUTHOR CONTRIBUTIONS

S. S. Virdee involved in conceptualization, data curation, funding acquisition, investigation, visualization, writing the original draft preparation, review and editing. **N. Z. Bashir** involved in formal analysis, investigation, visualization, writing the original draft preparation, review and editing. **M. Krstic** involved in data curation, investigation, visualization, review and editing. **M. M. Grant** involved in conceptualization, formal analysis, investigation, methodology, resources, supervision, review and editing. **J. Camilleri** involved in conceptualization, funding acquisition, supervision, review and editing. **P. R. Cooper** involved in conceptualization, funding acquisition, methodology, supervision, review and editing. **P. L. Tomson** involved in conceptualization, funding acquisition, supervision, review and editing.

ACKNOWLEDGEMENTS

This project has been supported by the following grants: (1) 2022 Glaxo-Smith-Kline Grant: Oral & Dental Research Trust; (2) 2020 Young Investigator Grant: European Society of Endodontology; (3) 2017 Annual Research Grant: British Endodontic Society. The first author was awarded the 2023 National Poster Prize at the British Endodontic Society Spring Scientific Meeting for the work presented in this manuscript.

CONFLICT OF INTEREST STATEMENT

The authors deny any conflicts of interest related to this study.

DATA AVAILABILITY STATEMENT

The data that support the findings of this study are available from the corresponding author upon reasonable request.

ORCID

Satnam S. Virdee https://orcid.org/0000-0002-8046-1805
Nasir Z. Bashir https://orcid.org/0000-0001-7416-7610
Milan Krstic https://orcid.org/0000-0002-3425-0484
Josette Camilleri https://orcid.org/0000-0003-3556-6365
Melissa M. Grant https://orcid.org/0000-0003-1154-7266
Paul R. Cooper https://orcid.org/0000-0003-1305-7287
Phillip L. Tomson https://orcid.org/0000-0001-5408-7744

REFERENCES

Alptekin, N.O., Ari, H., Haliloglu, S., Alptekin, T., Serpek, B. & Ataoglu, T. (2005) The effect of endodontic therapy on periapical exudate neutrophil elastase and prostaglandin-E2 levels. *Journal of Endodontia*, 31(11), 791–795.

Ataoğlu, T., Ungör, M., Serpek, B., Haliloğlu, S., Ataoğlu, H. & Ari, H. (2002) Interleukin-1beta and tumour necrosis factor-alpha levels in periapical exudates. *International Endodontic Journal*, 35(2), 181–185.

Ballal, V., Rao, S., Bagheri, A., Bhat, V., Attin, T. & Zehnder, M. (2017) MMP-9 in dentinal fluid correlates with caries lesion depth. *Caries Research*, 51(5), 460–465.

Brown, D.W.P. (2017) Paper points revisited: risk of cellulose fibre shedding during canal length confirmation. *International Endodontic Journal*, 50(6), 620–626.

Chapman, C.E. (1969) A microscopic study of the apical region ofhuman anterior teeth. *Journal of the British Endodontic Society*, 3(4), 52–58.

Connert, T., Judenhofer, M.S., Hülber-J, M., Schell, S., Mannheim, J.G., Pichler, B.J. et al. (2018) Evaluation of the accuracy of nine electronic apex locators by using micro-CT. *International Endodontic Journal*, 51(2), 223–232.

Corazza, B.J.M., Martinho, F.C., Khoury, R.D., Toia, C.C., Orozco, E.I.F., Prado, R.F. et al. (2021) Clinical influence of calcium hydroxide and N acetylcysteine on the levels of resolvins E1 and D2 in apical periodontitis. *International Endodontic Journal*, 54(1), 61–73.

da Cunha, P.C., Gomes, M.S., Della Bona, A., Vanni, J.R., Kopper, P.M. & de Figueiredo, J.A. (2008) Evaluation of two methods of measuring the absorbing capacity of paper points. *Dental Materials*, 24(3), 399–402.

Dummer, P.M., Hicks, R. & Huws, D. (1980) Clinical signs and symptoms in pulp disease. *International Endodontic Journal*, 13(1), 27–35.

Dummer, P.M., McGinn, J.H. & Rees, D.G. (1984) The position and topography of the apical canal constriction and apical foramen. *International Endodontic Journal*, 17(4), 192–198.

ESE. (2006) Quality guidelines for endodontic treatment: consensus report of the European Society of Endodontology. *International Endodontic Journal*, 39(12), 921–930.

Ferreira, L.G., Rosin, F.C. & Corrêa, L. (2016) Analysis of interleukin 17A in periapical abscess and granuloma lesions. *Brazilian Oral Research*, 30, S1806-83242016000100235.

Glickman, G.N. (2009) AAE Consensus Conference on Diagnostic Terminology: background and perspectives. *Journal of Endodontia*, 35(12), 1619–1620.

Grant, D.S., Kleinman, H.K., Goldberg, I.D., Bhargava, M.M., Nickoloff, B.J., Kinsella, J.L. et al. (1993) Scatter factor induces blood vessel formation in vivo. *Proceedings of the National Academy of Sciences of the United States of America*, 90(5), 1937–1941.

Grant, M.M., Taylor, J.J., Jaedicke, K., Creese, A., Gowland, C., Burke, B. et al. (2022) Discovery, validation, and diagnostic ability of multiple protein-based biomarkers in saliva and gingival crevicular fluid to distinguish between health and periodontal diseases. *Journal of Clinical Periodontology*, 49(7), 622–632.

Grga, D., Dzeletović, B., Damjanov, M. & Hajduković-Dragojlović, L. (2013) Prostaglandin E2 in apical tissue fluid and postoperative pain in intact and teeth with large restorations in two endodontic treatment visits. *Srpski Arhiv za Celokupno Lekarstvo*, 141(1–2), 17–21.

Hama, S., Takeichi, O., Hayashi, M., Komiyama, K. & Ito, K. (2006) Co-production of vascular endothelial cadherin and inducible nitric oxide synthase by endothelial cells in periapical granuloma. *International Endodontic Journal*, 39(3), 179–184.

Hartroth, B., Seyfahrt, I. & Conrads, G. (1999) Sampling of periodontal pathogens by paper points: evaluation of basic parameters. *Oral Microbiology and Immunology*, 14(5), 326–330.

Hasegawa, T., Venkata Suresh, V., Yahata, Y., Nakano, M., Suzuki, S., Suzuki, S. et al. (2021) Inhibition of the CXCL9-CXCR3 axis suppresses the progression of experimental apical periodontitis by blocking macrophage migration and activation. *Scientific Reports*, 11(1), 2613.

Inic-Kanada, A., Nussbaumer, A., Montanaro, J., Belij, S., Schlacher, S., Stein, E. et al. (2012) Comparison of ophthalmic sponges and extraction buffers for quantifying cytokine profiles in tears using Luminex technology. *Molecular Vision*, 18, 2717–2725.

Kabashima, H., Yoneda, M., Nagata, K., Hirofuji, T., Ishihara, Y., Yamashita, M. et al. (2001) The presence of chemokine receptor (CCR5, CXCR3, CCR3)-positive cells and chemokine (MCP1, MIP-1alpha, MIP-1beta, IP-10)-positive cells in human periapical granulomas. *Cytokine*, 16(2), 62–66.

Karamifar, K., Khayat, A., Mogharrabi, S., Rajaei, Y. & Saghiri, M.A. (2012) Effect of gravity and capillarity on human saliva penetration in coronally unsealed obturated root canals. *The Saudi Dental Journal*, 24(3–4), 157–162.

Kataria, N.G., Bartold, P.M., Dharmapatni, A.A., Atkins, G.J., Holding, C.A. & Haynes, D.R. (2010) Expression of tumor necrosis factor-like weak inducer of apoptosis (TWEAK) and its receptor, fibroblast growth factor-inducible 14 protein (Fn14), in healthy tissues and in tissues affected by periodontitis. *Journal of Periodontal Research*, 45(4), 564–573.

Katz, D.H., Robbins, J.M., Deng, S., Tahir, U.A., Bick, A.G., Pampana, A. et al. (2022) Proteomic profiling platforms head to head: leveraging genetics and clinical traits to compare aptamer- and antibody-based methods. *Science Advances*, 8(33), eabm5164.

Klausen, B., Helbo, M. & Dabelsteen, E. (1985) A differential diagnostic approach to the symptomatology of acute dental pain. *Oral Surgery, Oral Medicine, and Oral Pathology*, 59(3), 297–301.

Kwak, H.B., Lee, S.W., Jin, H.M., Ha, H., Lee, S.H., Takeshita, S. et al. (2005) Monokine induced by interferon-gamma is induced by receptor activator of nuclear factor kappa B ligand and is involved in osteoclast adhesion and migration. *Blood*, 105(7), 2963–2969.

Liu, W., Yu, J. & Zhou, H. (2003) Changes of prostaglandin E2 levels in periapical exudates after root canal treatment. *Hua Xi Kou Qiang Yi Xue Za Zhi*, 21(1), 39–40.

Lofthag-Hansen, S., Huumonen, S., Gröndahl, K. & Gröndahl, H.G. (2007) Limited cone-beam CT and intraoral radiography for the diagnosis of periapical pathology. *Oral Surgery, Oral Medicine, Oral Pathology, Oral Radiology, and Endodontics*, 103(1), 114–119.

Majeed, Z., Philip, K., Alabsi, A.M., Pushparajan, S. & Swaminathan, D. (2016) Identification of gingival Crevicular fluid sampling, analytical methods, and oral biomarkers for the diagnosis and monitoring of periodontal diseases: a systematic review. *Disease Markers*, 2016, 1804727.

Mao, Y.J., Sheng, X.R. & Pan, X.M. (2007) The effects of NaCl concentration and pH on the stability of hyperthermophilic protein Ssh10b. *BMC Biochemistry*, 8, 28.

Martinho, F.C., Nascimento, G.G., Leite, F.R., Gomes, A.P., Freitas, L.F. & Camões, I.C. (2015) Clinical influence of different intracanal medications on Th1-type and Th2-type cytokine responses in apical periodontitis. *Journal of Endodontia*, 41(2), 169–175.

Martinho, F.C., Teixeira, F.F., Cardoso, F.G., Ferreira, N.S., Nascimento, G.G., Carvalho, C.A. et al. (2016) Clinical investigation of matrix metalloproteinases, tissue inhibitors of matrix metalloproteinases, and matrix metalloproteinase/tissue inhibitors of matrix metalloproteinase complexes and their networks in apical periodontitis. *Journal of Endodontia*, 42(7), 1082–1088.

Marton, I.J. & Kiss, C. (1993) Characterization of inflammatory cell infiltrate in dental periapical lesions. *International Endodontic Journal*, 26(2), 131–136.

Márton, I.J. & Kiss, C. (2000) Protective and destructive immune reactions in apical periodontitis. *Oral Microbiology and Immunology*, 15(3), 139–150.

Márton, I.J. & Kiss, C. (2014) Overlapping protective and destructive regulatory pathways in apical periodontitis. *Journal of Endodontia*, 40(2), 155–163.

Matsuo, T., Ebisu, S., Nakanishi, T., Yonemura, K., Harada, Y. & Okada, H. (1994) Interleukin-1 alpha and interleukin-1 beta periapical exudates of infected root canals: correlations with the clinical findings of the involved teeth. *Journal of Endodontia*, 20(9), 432–435.

Mente, J., Petrovic, J., Gehrig, H., Rampf, S., Michel, A., Schürz, A. et al. (2016) A prospective clinical pilot study on the level of matrix metalloproteinase-9 in dental pulpal blood as a marker for the state of inflammation in the pulp tissue. *Journal of Endodontia*, 42(2), 190–197.

Nagendrababu, V., Duncan, H.F., Fouad, A.F., Kirkevang, L.L., Parashos, P., Pigg, M. et al. (2023) PROBE 2023 guidelines for reporting observational studies in Endodontics: a consensus-based development study. *International Endodontic Journal*, 56(3), 308–317.

Nagendrababu, V., Murray, P.E., Ordinola-Zapata, R., Peters, O.A., Rôças, I.N., Siqueira, J.F., Jr. et al. (2021) PRILE 2021 guidelines for reporting laboratory studies in Endodontology: a consensus-based development. *International Endodontic Journal*, 54(9), 1482–1490.

Nair, P.N. (2004) Pathogenesis of apical periodontitis and the causes of endodontic failures. *Critical Reviews in Oral Biology and Medicine*, 15(6), 348–381.

Nakanishi, K., Yoshimoto, T., Tsutsui, H. & Okamura, H. (2001) Interleukin-18 regulates both Th1 and Th2 responses. *Annual Review of Immunology*, 19, 423–474.

Nonaka, C.F., Maia, A.P., Nascimento, G.J., de Almeida, F.R., Batista de Souza, L. & Galvão, H.C. (2008) Immunoexpression of vascular endothelial growth factor in periapical granulomas, radicular cysts, and residual radicular cysts. *Oral Surgery, Oral Medicine, Oral Pathology, Oral Radiology, and Endodontics*, 106(6), 896–902.

Ohgi, K., Kajiya, H., Goto, T.K., Okamoto, F., Yoshinaga, Y., Okabe, K. et al. (2018) Toll-like receptor 2 activation primes and upregulates osteoclastogenesis via lox-1. *Lipids in Health and Disease*, 17(1), 132.

Patel, S., Dawood, A., Mannocci, F., Wilson, R. & Pitt Ford, T. (2009) Detection of periapical bone defects in human jaws using cone beam computed tomography and intraoral radiography. *International Endodontic Journal*, 42(6), 507–515.

Pezelj-Ribarić, S., Magasić, K., Prpić, J., Miletić, I. & Karlović, Z. (2007) Tumor necrosis factor-alpha in peripical tissue exudates of teeth with apical periodontitis. *Mediators of Inflammation*, 2007, 69416.

Pumarola-Suñé, J., Solá-Vicens, L., Sentís-Vilalta, J., Canalda-Sahli, C. & Brau-Aguadé, E. (1998) Absorbency properties of different brands of standardized endodontic paper points. *Journal of Endodontia*, 24(12), 796–798.

Rechenberg, D.K., Bostanci, N., Zehnder, M. & Belibasakis, G.N. (2014) Periapical fluid RANKL and IL-8 are differentially regulated in pulpitis and apical periodontitis. *Cytokine*, 69(1), 116–119.

Reisinger, K., Kaufmann, R. & Gille, J. (2003) Increased Sp1 phosphorylation as a mechanism of hepatocyte growth factor (HGF/SF)-induced vascular endothelial growth factor (VEGF/VPF) transcription. *Journal of Cell Science*, 116(Pt 2), 225–238.

Repeke, C.E., Ferreira, S.B., Jr., Claudino, M., Silveira, E.M., de Assis, G.F., Avila-Campos, M.J. et al. (2010) Evidences of the cooperative role of the chemokines CCL3, CCL4 and CCL5 and its receptors CCR1+ and CCR5+ in RANKL+ cell migration throughout experimental periodontitis in mice. *Bone*, 46(4), 1122–1130.

Ricucci, D. & Bergenholtz, G. (2004) Histologic features of apical periodontitis in human biopsies. *Endodontic Topics*, 8(1), 68–87.

Safavi, K.E. & Rossomando, E.F. (1991) Tumor necrosis factor identified in periapical tissue exudates of teeth with apical periodontitis. *Journal of Endodontia*, 17(1), 12–14.

Sette-Dias, A.C., Maciel, K.F., Abdo, E.N., Brito, L.C.N., Carvalho, M.A.R., Vieira, L.Q. et al. (2016) Cytokine expression in patients hospitalized for severe odontogenic infection in Brazil. *Journal of Endodontia*, 42(5), 706–710.

Shimauchi, H., Miki, Y., Takayama, S., Imai, T. & Okada, H. (1996) Development of a quantitative sampling method for periapical exudates from human root canals. *Journal of Endodontia*, 22(11), 612–615.

Shimauchi, H., Takayama, S., Imai-Tanaka, T. & Okada, H. (1998) Balance of interleukin-1 beta and interleukin-1 receptor antagonist in human periapical lesions. *Journal of Endodontia*, 24(2), 116–119.

Silva, T.A., Garlet, G.P., Fukada, S.Y., Silva, J.S. & Cunha, F.Q. (2007) Chemokines in oral inflammatory diseases: apical periodontitis and periodontal disease. *Journal of Dental Research*, 86(4), 306–319.

Šimundić, A.M. (2009) Measures of diagnostic accuracy: basic definitions. *EJIFCC*, 19(4), 203–211.

Sorsa, T., Alassiri, S., Grigoriadis, A., Räisänen, I.T., Pärnänen, P., Nwhator, S.O. et al. (2020) Active MMP-8 (aMMP-8) as a grading and staging biomarker in the periodontitis classification. *Diagnostics*, 10(2), 61.

Steinitz, M. (2000) Quantitation of the blocking effect of tween 20 and bovine serum albumin in ELISA microwells. *Analytical Biochemistry*, 282(2), 232–238.

Teixeira, F.F.C., Cardoso, F.G.R., Ferreira, N.S., Corazza, B.J.M., Valera, M.M.C., Nascimento, G.G. et al. (2022) Effects of calcium hydroxide Intracanal medications on T helper (Th1, Th2, Th9, Th17, and Tfh) and regulatory T (Treg) cell cytokines in apical periodontitis: a CONSORT RCT. *Journal of Endodontia*, 48(8), 975–984.

Tsai, C.H., Huang, F.M. & Chang, Y.C. (2008) Immunohistochemical localization of oncostatin M in epithelialized apical periodontitis lesions. *International Endodontic Journal*, 41(9), 772–776.

Virdee, S.S., Butt, K., Grant, M., Camilleri, J., Cooper, P.R. & Tomson, P.L. (2019) A systematic review of methods used to sample and analyse periradicular tissue fluid during root canal treatment. *International Endodontic Journal*, 52(8), 1108–1127.

Wahlgren, J., Salo, T., Teronen, O., Luoto, H., Sorsa, T. & Tjäderhane, L. (2002) Matrix metalloproteinase-8 (MMP-8) in pulpal and periapical inflammation and periapical root-canal exudates. *International Endodontic Journal*, 35(11), 897–904.

Weber, M., Ries, J., Büttner-Herold, M., Geppert, C.I., Kesting, M. & Wehrhan, F. (2019) Differences in inflammation and bone resorption between apical granulomas, radicular cysts, and dentigerous cysts. *Journal of Endodontia*, 45(10), 1200–1208.

Wik, L., Nordberg, N., Broberg, J., Björkesten, J., Assarsson, E., Henriksson, S. et al. (2021) Proximity extension assay in combination with next-generation sequencing for high-throughput proteome-wide analysis. *Molecular & Cellular Proteomics*, 20, 100168.

Yakar, N., Guncu, G.N., Akman, A.C., Pınar, A., Karabulut, E. & Nohutcu, R.M. (2019) Evaluation of gingival crevicular fluid and peri-implant crevicular fluid levels of sclerostin, TWEAK, RANKL and OPG. *Cytokine*, 113, 433–439.

Youden, W.J. (1950) Index for rating diagnostic tests. *Cancer*, 3(1), 32–5.

Zehnder, M. & Belibasakis, G.N. (2022) A critical analysis of research methods to study clinical molecular biomarkers in Endodontic research. *International Endodontic Journal*, 55(Suppl 1), 37–45.

Zehnder, M., Rechenberg, D.K., Bostanci, N., Sisman, F. & Attin, T. (2014) Comparison of vehicles to collect dentinal fluid for molecular analysis. *Journal of Dentistry*, 42(8), 1027–1032.

Zhi, J., Yu, D., Yuan, D. & Chen, J. (2017) Interleukin-17 in apical exudates of periapical periodontitis treated with minocycline controlled-release formulation. *Chinese Journal of Tissue Engineering Research*, 21(10), 1508–1513.

Zhou, H., Yuen, P.S., Pisitkun, T., Gonzales, P.A., Yasuda, H., Dear, J.W. et al. (2006) Collection, storage, preservation, and normalization of human urinary exosomes for biomarker discovery. *Kidney International*, 69(8), 1471–1476.

SUPPORTING INFORMATION

Additional supporting information can be found online in the Supporting Information section at the end of this article.

How to cite this article: Virdee, S.S., Bashir, N.Z., Krstic, M., Camilleri, J., Grant, M.M., Cooper, P.R. et al. (2023) Periradicular tissue fluid-derived biomarkers for apical periodontitis: An *in vitro* methodological and *in vivo* cross-sectional study. *International Endodontic Journal*, 00, 1–19. Available from: https://doi.org/10.1111/iej.13956